# Damping of metallic wool with embedded rigid body motion amplifiers

**Charles E. Lord[1], Ning Tang[2], Jem A. Rongong[3]**

[1,2,3]*University of Sheffield, Department of Mechanical Engineering, Dynamics Research Group, Mappin Street, Sheffield, S1 3JD, United Kingdom*

## ABSTRACT

The use of entangled metallic wires as vibrational dampers and shock isolators is of interest in a variety of applications. By taking advantage of the frictional contact between the contiguous wires, it has been shown that significant amounts of energy dissipation can be achieved. The amount of energy dissipation is highly dependent on many factors with one in particular being the excitation amplitude. When the excitation amplitude is low, a combination of the number of contact points, in which have relative motion, and the contact pressure are lessened often leading to a sacrifice in energy dissipation. In this paper, spherical metallic rigid bodies are embedded within metallic wool. These rigid bodies act as motion amplifiers in which, locally within the metallic wool, amplify the excitation amplitude leading to an increase in vibrational damping. Presented are experimental modal results from various metallic wool/embedded rigid body arrangements within a prismatic hollow aluminium tube. It is found that the incorporation of the embedded rigid bodies into the steel wool significantly improves the damping within the system. It is demonstrated that an increase in damping by 2328% has been achieved at only a 3.8% penalty in mass. It is found that the level of damping from the embedded rigid bodies depends not only on the excitation amplitude but their quantity and the accompanying steel wool configuration. A finite element procedure coupled with an analytical model is proposed which accounts for the strain energy produced within the steel wool to estimate the damping effect that this filler material has on the behaviour of the overall structure. The model treats the metallic wool/rigid sphere combination as a homogeneous equivalent solid with amplitude dependent damping properties, thereby reducing the complexities of the physics-based model while still providing an estimate of the vibrational damping while in the frequency domain.

**Keywords:** *vibration control, friction damping, entangled metal wire, tuned mass damper, metamaterial*

## 1 INTRODUCTION

Vibration control of structures is an area that has received notable consideration, both in industry and in research, over the past several decades. Every structure encounters some kind of dynamic loading. This loading can roughly be categorised into two main groups: structures that receive negligible vibration and acoustic loads, which we refer to as static structures, and structures where the dynamic and acoustic loads cannot be ignored, which we refer to as dynamic structures. In these dynamic structures, there is a reliance on damping to dissipate a portion of the energy therefore reducing the dynamic response of the structure to an acceptable limit. Dissipating this energy effectively is not a trivial task.

A material that has gained attention for vibration damping, due to its relatively high damping capacity, is entangled metal wire (also commonly referred to as knitted mesh or metal rubber [1]).

[1] Lecturer, *c.lord@sheffield.ac.uk

[2] PhD Student, ntang1@sheffield.ac.uk

[3] Senior Lecturer, j.a.rongong@sheffield.ac.uk



* Corresponding author

Entangled metal wire is a porous material comprised of tangled metallic helical wire manufactured via a combination of processes including wire drawing, weaving, and compression molding [2]. When loaded, the individual wires of these materials rub against each other dissipating energy through Coulombic (friction) damping. For such materials, they can require large strains to be effective in providing vibrational damping. When the amplitude is not large enough, the wires can remain locked together therefore either limiting or not allowing relative motion leading to a reduction in damping.

In this paper, the incorporation of spherical rigid body motion amplifiers (RBMAs) embedded into commercial grade steel wool is explored. This new material is exposed to forced flexural bending vibrations using an electrodynamic shaker for various excitation amplitudes and various configurations of steel wool pre-stressing and particle distribution and size. A comparison in made between the steel wool with and without the introduction of the motion amplifiers.

## 2 EXPERIMENTS AND SETUP

The objective for the experiments was to evaluate the effectiveness, for modes 1 and 2, from flexural vibrational damping, for the steel wool with the addition of RBMAs. A prismatic hollow aluminium tube with an outer cross-section of 38mm x 38mm with a wall thickness of 1.5mm was used to test the material. The tube was constrained to represent cantilever boundary conditions with an unconstrained length of 700mm. The steel wool configurations maintained a constant nominal width of 35mm and length of 200mm while the thickness varied.

The start of the steel wool was positioned in the tube 180mm from the fixed end and constrained by its reaction force (to compressive loads) in addition to internal stop plates located at both ends of the steel wool. Forced vibration experiments were performed using an electrodynamic shaker to excite the tube and steel wool combinations. Receptance frequency response functions (FRFs) were measured and used to extract modal parameters (natural frequencies and damping ratios). The position of the shaker, test sample, and accelerometer were carefully positioned to avoid any modal nodes for flexural modes 1 and 2 (in the direction of excitation). The modal node locations were estimated from a modal analysis, using finite elements (FEs), for both the empty tube and the tube with the largest additional mass from the steel wool with RBMA configurations. The test setup and FE mode shapes are shown in Fig. 1. It is demonstrated that the largest additional mass, compared to the empty tube, has little significance for mode 1 while mode 2 shows a large difference. This is an important characteristic as this will change the modal strain energy and affect the effectiveness of the RBMAs.

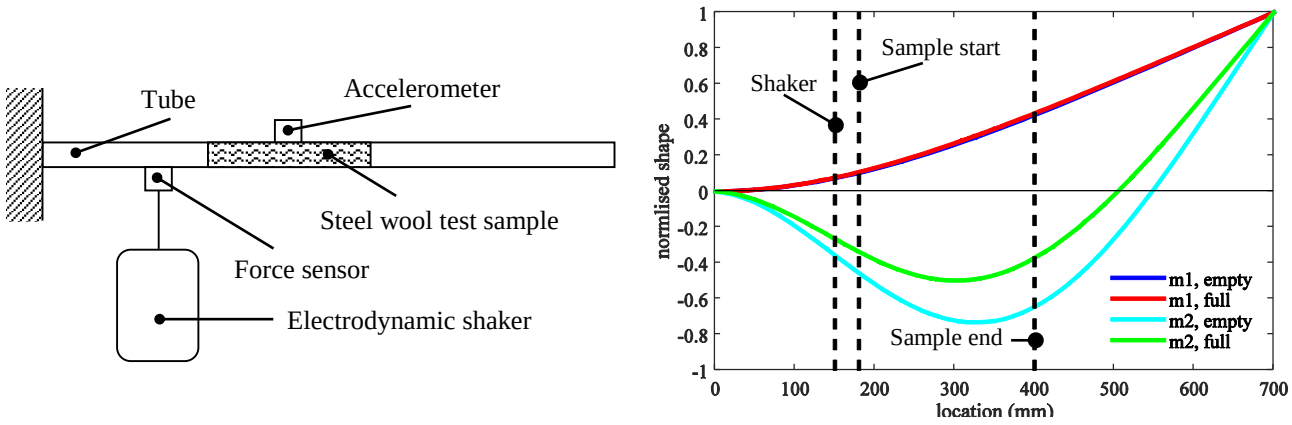


(a) (b)

*Figure 1 –* (a) *experimental setup and* (b) *shaker and sample locations relative to FE mode shapes.*

Three different configurations of experiments were completed for the testing: the empty tube, tube with steel wool, and the tube with steel wool and RBMAs. Results from only an extra fine grade of steel wool (0.025mm nominal wire diameter) and the spherical steel RBMAs of 10mm diameter are

discussed in this paper. The steel wool is supplied on a roll with the thickness being nominally 10.3mm. Layers are produced by folding a continuous length of the steel wool onto itself in a zig-zag pattern with the number of layers increasing in the thickness/excitation direction. The RBMAs are inserted into the steel wool by evenly distributing them between the layers. Care is taken so that the RBMAs are not too close to an edge and become dislodged during vibratory loading.

Each test consists of FRF measurements from an initial random excitation to identify the resonance frequencies for bending modes 1 and 2. Once these were identified, high resolution stepped sine tests were completed encompassing modes 1 and 2 separately. These FRFs were then used to compare the natural frequencies and damping ratios or dissipated energy for each of the configurations.

## 2.1 Empty tube

During damping measurements, it is necessary to understand the contribution that other sources may provide to the overall system damping; in the case for these tests, the clamping. Several tests were completed with varying torque being applied to the clamp at the fixed end of the tube. Even though much effort went into trying to get an idealised constraint, this was difficult to achieve fully for the damping. The amplitude dependent mode 1 and mode 2 natural frequencies and damping ratios from the empty tube are provided in Fig. 2.

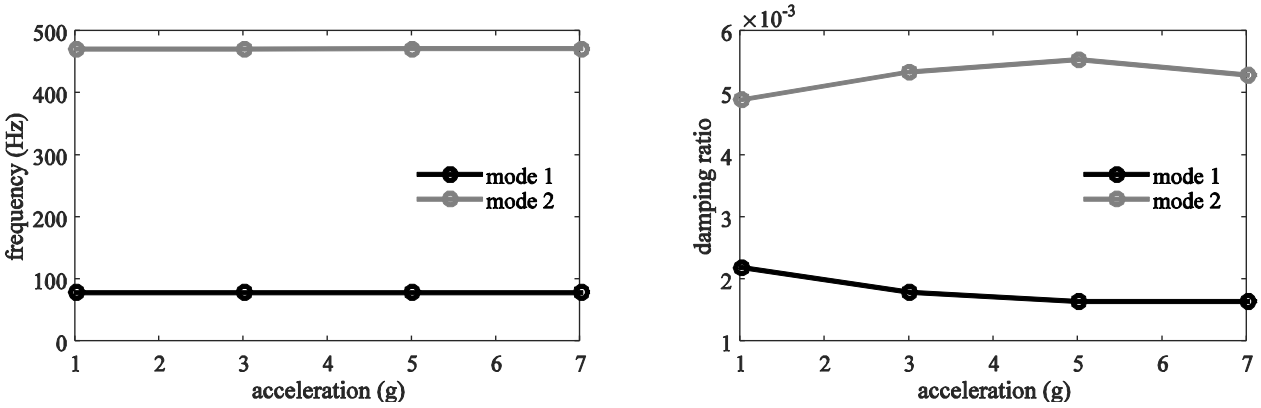


(a) (b)

*Figure 2 – Modes 1 and 2 for empty tube acceleration dependent* (a) *natural frequencies and* (b) *damping ratios.*

## 2.2 Tube containing steel wool

To get a better understanding how steel wool behaves, when used as a vibration damper, and to compare to the empty tube, the tube was stuffed with extra fine steel wool as depicted in Fig. 1a using 4, 6, and 8 layer configurations. Each configuration is such that a compression/compaction is required therefore the steel wool is in contact with all interior sides of the tube. The purpose of the various layer quantity was to compare the effect that the compaction/prestress has on the natural frequency and damping ratio. From Fig. 3, it is demonstrated for both modes 1 and 2 that the natural frequency has a minimal change. When increasing the number of layers, there is a competition between the increased mass, which would normally reduce the natural frequency, and the increased stiffness, which would normally increase the natural frequency. The minimal change is most likely due to the level of mass and stiffness change being a relatively small percent of the total system. One interesting feature however, is that for mode 1, the damping ratio actually decreases as the layer number increases. This can be attributed to the ‘locking’ of the wires in the steel wool as the compaction increases. However, the same does not hold for mode 2, particularly for the 6 layer configuration where a jump in damping ratio exists. The FRF for this configuration identified an additional

resonance at 448Hz which could be responsible for poor modal parameter estimation from using a local single degree of freedom curve fit thereby creating a poor estimation of the damping due to a heavy modal density (strong coupling).

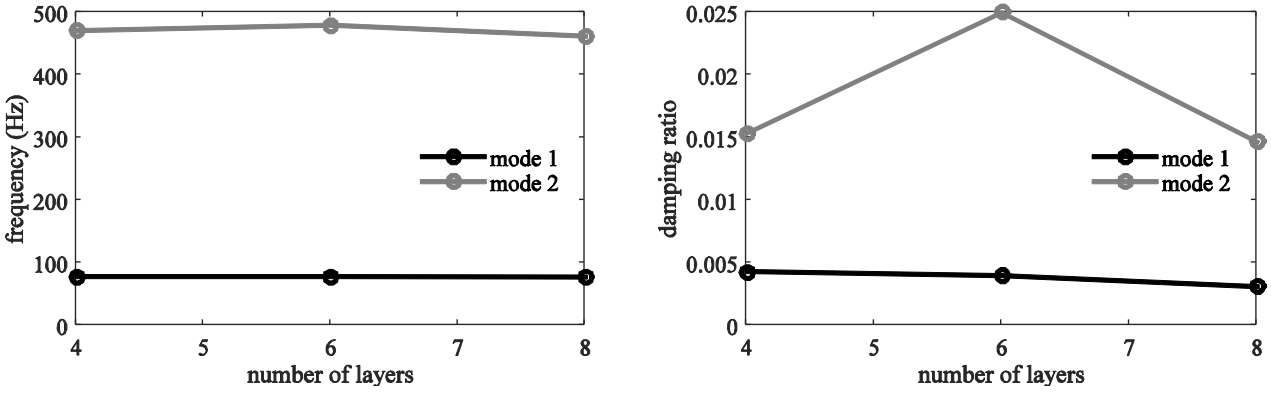


(a) (b)

*Figure 3 –Modes 1 and 2 compaction/prestress dependent* (a) *natural frequencies and* (b) *damping ratios for various number of layers of extra fine steel wool subjected to 1g harmonic loading.*

The 4 layer configuration was additionally used to demonstrate the effect that the excitation level has on the steel wool. Fig. 4 depicts the excitation amplitude dependent frequency and damping. It is shown that as the excitation has an insignificant effect on the natural frequency for both modes 1 and 2. It can be noticed that as the acceleration increases the damping ratio decreases for mode 1 but increases for mode 2. This is believed to be due to small amounts of sliding of the steel wool inside the tube from increased axial accelerations, due to the mode shape curvature, in mode 2.

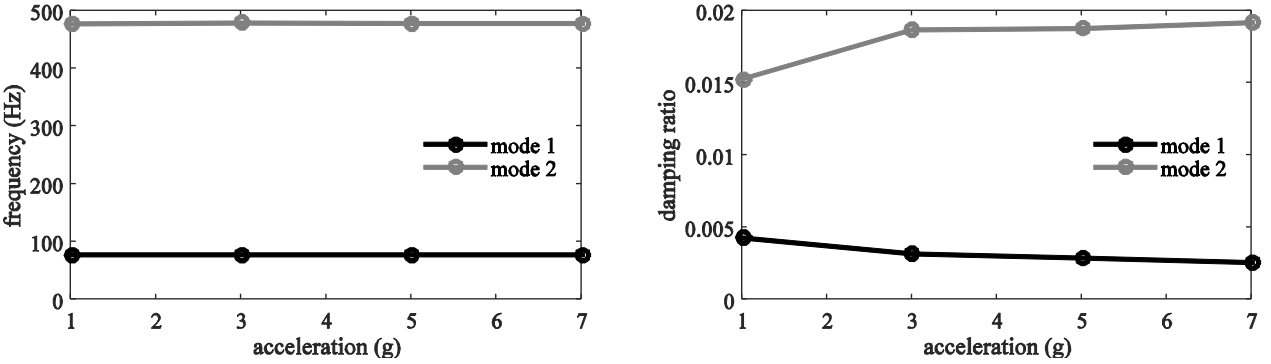


(a) (b)

*Figure 4 – Modes 1 and 2 amplitude dependent* (a) *natural frequencies and* (b) *damping ratios for 4 layers of extra fine steel wool.*

## 2.3 Tube with steel wool and RBMAs

As discussed previously, entangled metal wires can require a substantial strain to provide a significant level of vibration damping. In this section, the incorporation of RBMAs are included to exacerbate the deformation in the steel wool locally to increase the dissipated energy. To gain a better understanding of how the RBMAs interact with the steel wool, the attributes of nonlinearity from various driving amplitudes, the quantity and distribution of the RBMAs, and compaction/prestress is focused on.

### 2.3.1 Nonlinearity

Steel wool alone is a nonlinear material due to its wire-to-wire frictional interactions. When the RBMAs are added to the steel wool this nonlinearity changes. This is partially due to how the stiffness between the RBMAs and steel wool is altered from the deformation changes. Other factors include the complex motion of the RBMAs in the steel wool and the presence of friction between the RBMAs and the steel wool. The properties for each test configuration are provided in Table 1.

*Table 1: Properties for Test ID 001*

| Test ID | mode | excitation (g's) | *n* steel wool layers | *n* RBMA layers | *n* RBMAs per layer | total RBMAs | compaction | RBMA wt. (g) | steel wool wt. | total wt. |
|---|---|---|---|---|---|---|---|---|---|---|
| 001 | 1 | 1 | 4 | 2 | 20 | 40 | 17.7% | 164.64 | 24.33 | 188.97 |
| | | 3 | | | | | | | | |
| | | 5 | | | | | | | | |
| | | 7 | | | | | | | | |
| | 2 | 1 | 4 | 2 | 20 | 40 | 17.7% | 164.64 | 24.33 | 188.97 |
| | | 3 | | | | | | | | |
| | | 5 | | | | | | | | |
| | | 7 | | | | | | | | |

Fig. 5 demonstrates the nonlinearity that is dependent on the excitation amplitude. For mode 1, as the acceleration is increased, the natural frequency increases slightly. However, for mode 2, the opposite is true. One possible reason for this difference could be from the steel wool reaching a sloshing type mode within the tube. A similar contradictory behaviour is observed in Fig. 5b. For mode 1, as the acceleration increases, there is an initial increase in damping followed by a decrease. For mode 1, the opposite is present. As the acceleration increases, the damping ratio decreases and then increases, mirroring mode 1.

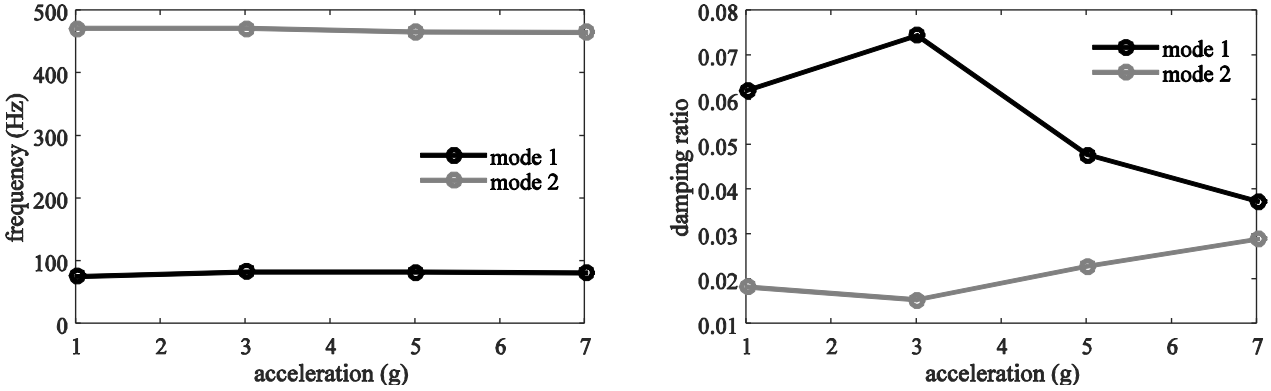


(a) (b)

*Figure 5 – Modes 1 and 2 nonlinearity for* (a) *natural frequencies and* (b) *damping ratios for 4 layers of extra fine steel wool excited at various accelerations.*

### 2.3.2 RBMA quantity and distribution

Both the quantity and the distribution of the RBMAs are parameters that can be easily changed between the experiments. The steel wool and RBMAs configurations used are provided in Table 2.

*Table 2: Properties for Test IDs 003, 006, and 007*

| Test ID | mode | excitation (g's) | *n* steel wool layers | *n* RBMA layers | *n* RBMA per layer | total RBMAs | compaction | RBMA wt. (g) | steel wool wt. | total wt. |
|---|---|---|---|---|---|---|---|---|---|---|
| 003 | 1<br>2 | 1 | 6 | 2 | 10 | 20 | 76.6% | 82.32 | 34.40 | 116.72 |
| 006 | 1<br>2 | 1 | 6 | 2 | 20 | 40 | 76.6% | 164.64 | 34.40 | 199.04 |
| 007 | 1<br>2 | 1 | 6 | 3 | 13, 14, 13 | 40 | 76.6% | 164.64 | 34.40 | 199.04 |

The quantity of RBMAs not only controls the additional mass of the system but also the density of the RBMAs to the steel wool. It is important when determining the quantity of RBMAs that an 'overcrowding' does not occur and the RBMAs actually become counterproductive. The FRFs from mode 1 are very clean and well separated unlike those from mode 2 (shown in Fig. 6a). Therefore a more appropriate method would be to estimate the power dissipation using a power flow method [3,4]. The method, at a top level, works by taking the inverse Fourier transform of the FRF and then taking the autocorrelation for the half waveform for a set bandwidth. The autocorrelation is then squared to arrive at the power spectral density which is then averaged over the length of the PSD data points. Although the FRFs containing mode 1 were well separated from other modes, the power flow method was applied to these also for a direct comparison to mode 2. The configurations considered for comparison of the quantity of RBMAs is for Test IDs 003 and 006. It is shown in Fig. 6b that the power flow between Test IDs 003 and 006 vary from the RBMAs and there is a difference in between respective modes 1 and 2. As the quantity of RBMAs is increased, the power dissipation also increases. This is expected as the total strain energy has increased. Also, mode 1 has a consistently higher power dissipation as compared to mode 2. This is in part an attribute of mode 1 having a higher velocity than mode 2, as a constant acceleration is used. By comparing Test IDs 006 and 007, the effect that the distribution of RBMAs has on the system is shown. For mode 1 the difference is negligible while for mode 2 there is a noticeable difference. When comparing modes 1 and 2 for the respective Test ID, there is minimal difference for 006 while there is a substantial difference for mode 2.

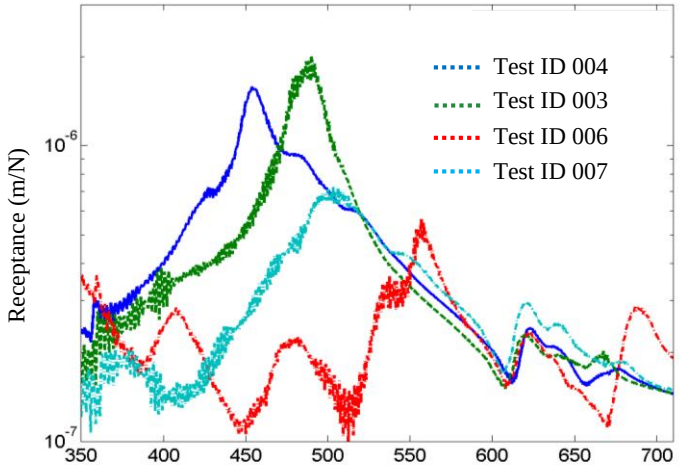


(a)

| Mode | Test ID | $f_n$ (Hz) | $Q$ (W) |
|---|---|---|---|
| 1 | 003 | 74.9 | 0.028 |
| | 006 | 71.7 | 0.054 |
| | 007 | 72.1 | 0.052 |
| 2 | 003 | 484 | 0.017 |
| | 006 | 480 | 0.050 |
| | 007 | 505 | 0.036 |

(b)

*Figure 6 – Test IDs 003, 006, and 007 (a) encompassed mode 2 FRFs and (b) modes 1 and 2 natural frequencies and average power dissipation for 1g harmonic loading using fine steel wool.*

### 2.3.3 Steel wool and RBMA compaction/prestress

One parameter in particular the performance of entangled metal wire is very sensitive to is the compaction/prestress. This also is valid for steel wool. A total of 4 test configurations were considered for these tests as outlined in Table 3. The Test IDs should be compared in pairs; 002 with 003 and

004 with 005. Both pairs compare the compaction between 4 and 6 layers. The FRFs from mode 2 for each of the experiments is inconclusive to extract modal parameters from easily. A better method for comparison is by calculating the power dissipated using the power flow method. To further this, it will also be used for mode 1 to compare directly with mode 2. For Test ID 002, for modes 1 and 2 there is no obvious difference. However, for Test ID 003, there is a considerable difference between modes 1 and 2. One possible explanation for this disagreement between Test IDs 002 and 003 is that for Test ID 003 mode 2, as the compaction is greater, the shear strains are permitted into the steel wool without slipping.

Comparing Test IDs 004 and 005, for the power dissipation there is no difference between modes 1 and 2 for Test ID 004. There is a noticeable decrease in power dissipation though for Test ID 005. This decrease is believed to be for the same reason as in Test ID 003 between mode 1 and 2. It is also noticed that for the Test IDs with the higher compaction, there is an expected higher weight. Again, the mass and stiffness compete against each other and is shown that the ratio of stiffness-to-weight is <1 decreasing the natural frequencies for mode 1. It is inconclusive as to the frequency shifts for mode 2 for each of the Test IDs. This is potentially due to the change in mode shape therefore drastically changing the stiffness of the system.

*Table 3: Properties for Test IDs 002 - 005*

| Test ID | mode | excitation (g's) | *n* steel wool layers | *n* RBMA layers | *n* RBMAs per layer | total RBMAs | compaction | RBMA wt. (g) | steel wool wt. | total wt. |
|---|---|---|---|---|---|---|---|---|---|---|
| 002 | 1 | 1 | 4 | 2 | 10 | 20 | 17.7% | 82.32 | 24.33 | 106.65 |
| | 2 | | | | | | | | | |
| 003 | 1 | 1 | 6 | 2 | 10 | 20 | 76.6% | 82.32 | 34.40 | 116.72 |
| | 2 | | | | | | | | | |
| 004 | 1 | 1 | 4 | 1 | 20 | 20 | 17.7% | 82.32 | 24.33 | 106.65 |
| | 2 | | | | | | | | | |
| 005 | 1 | 1 | 6 | 1 | 20 | 20 | 76.6% | 82.32 | 34.40 | 116.72 |
| | 2 | | | | | | | | | |

| Mode | Test ID | $f_n$ (Hz) | $Q$ (W) |
|---|---|---|---|
| 1 | 002 | 80.0 | 0.024 |
| | 003 | 74.9 | 0.028 |
| | 004 | 80.3 | 0.024 |
| | 005 | 75.2 | 0.024 |
| 2 | 002 | 466 | 0.024 |
| | 003 | 484 | 0.017 |
| | 004 | 474 | 0.024 |
| | 005 | 460 | 0.020 |

*Figure 7 – Modes 1 and 2 natural frequencies and average power dissipation for Test IDs 002-005.*

### 2.3.4 Effectiveness of RBMAs

The empty tube, tube with steel wool, and tube with steel wool and RBMAs (Test ID 001) have been measured for their mode 1 and 2 natural frequencies and their associated damping ratios. A comparison is made between each of them to understand the effectiveness of the introduction of the embedded RBMAs. Each test containing steel wool consists of 4 layers of extra fine grade. Each test was excited at various accelerations; the steady-state response modal parameters are used as a comparison. The RBMAs used are steel with a spherical diameter of 10mm. A comparison for flexural modes 1 and 2 for the natural frequencies and damping ratios is given in Fig. 8.

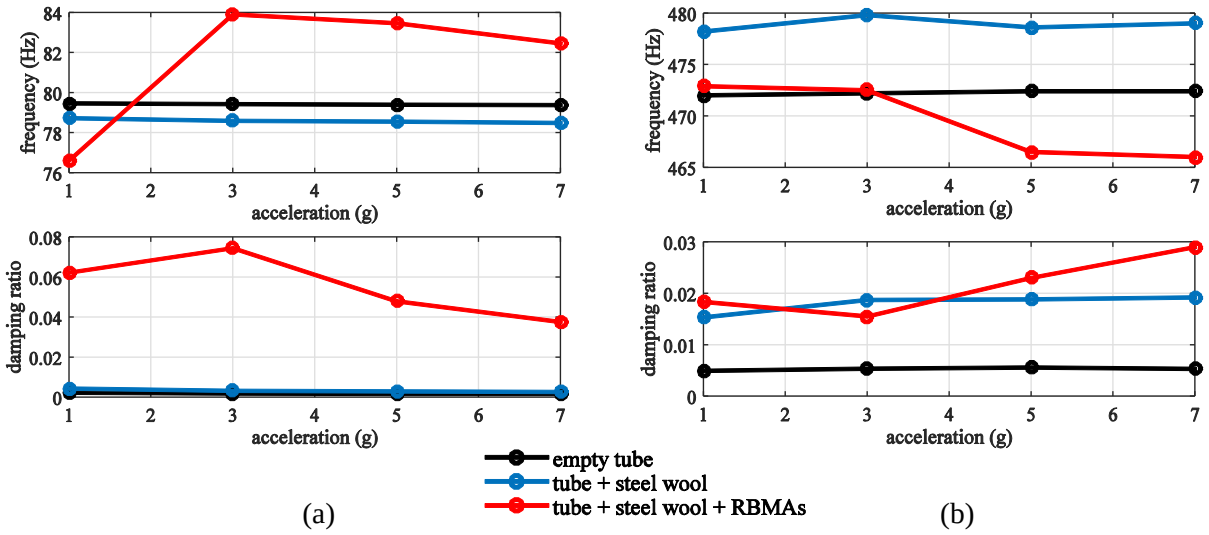


*Figure 8 – Effectiveness of RBMAs embedded into steel wool for acceleration dependent natural frequency and damping ratio for* (a) *mode 1 and* (b) *mode 2.*

For modes 1 and 2, the frequency shift, between the empty tube and the tube with steel wool, has a consistent offset and is nearly constant throughout the various excitation amplitudes. However, for the tube with steel wool and RBMAs, with respect to the excitation amplitude for mode 1, the natural frequency initially increases followed by a decrease while for mode 2 there is a decrease as the excitation amplitude is increased, but at different rates. It is believed that the reason for the decrease in natural frequency, for modes 1 and 2, is that at low accelerations the RBMAs activate the damping of the steel wool to a low level where the overall stiffness of the steel wool is larger than when the excitation is high. Additionally this could also be caused from RBMA migration, within the steel wool, into an agglomerate where the RBMAs settle biasedly positioned toward the free end of the tube reducing the system stiffness.

For modes 1 and 2, the damping ratio between the empty tube and the tube with steel wool has a consistent offset and is nearly constant throughout the various excitation amplitudes. For the tube with steel wool and RBMAs, there is a fluctuation in the damping ratio. This is due to the fluctuating change in loss factor of the steel wool which is common with frictional damping. For the damping ratio, for mode 1, the tube alone is the lowest followed by the tube with steel wool and finally the tube with steel wool and RBMAs. The RBMAs make a large difference to the damping (up to 2328%) with a minimal impact on the overall added mass (3.8%) of the system. For mode 2, the damping capacity for each configuration follows the same trend as mode 1, apart from at 3g.

## 3 SEMI-ANALYTICAL NUMERICAL MODEL

To represent the RBMAs in the steel wool, a semi-analytical-numerical model is proposed. The model relies on iterative cross-coupling between a finite element (FE) model and an analytical model. The FE model is firstly used to estimate the acceleration response where the RBMAs are located within the structure. Due to the routine (downstream) utilising a linear modal analysis, the acceleration response is achieved with a frequency-domain harmonic analysis. These responses are then used in the analytical model to estimate the strain energy, $U_1$, from the RBMAs. From the harmonic analysis, the total strain energy, $U$, for the steel wool and RBMAs is identified. Using the strain energies, the vibrational loss factor, $\eta_1$, is calculated for the steel wool and RBMAs using the modal strain energy (MSE) method defined as

$$\eta_1 = \eta\left(\frac{U_1}{U}\right), \tag{1}$$

$$U = \sum \left[ V_{es} U_{es} \left( \sum_{1}^{n} V_{es} \right)^{-1} \right], \tag{2}$$

where $\eta$ is the experimental vibrational loss factor for the steel wool, $U_{es}$ is the element strain energy for the steel wool, $V_{es}$ is the volume for element in the steel wool, and $n$ is the number of elements. Next, a damped modal analysis is completed to estimate the system total strain energy, $U_t$; separating the strain energy for the steel wool and RBMAs from the system total strain energy. Lastly, using the MSE, the system loss factor, $\eta_2$, is calculated as

$$\eta_2 = \eta_1 \left( \frac{U}{U_t} \right), \tag{3}$$

$$U_t = \sum \left[ V_{et} U_{et} \left( \sum_{1}^{n} V_{et} \right)^{-1} \right], \tag{4}$$

where $U_{et}$ is the element strain energy for the system and $V_{et}$ is the volume for each element in the system. Once $U_t$ is calculated, it is placed back into the harmonic analysis to ascertain an improved response accuracy. The steps are all repeated and this process is looped through until the change in $U_t$ is within a tolerance. The procedural process flow for the models is summarised in Fig. 9.

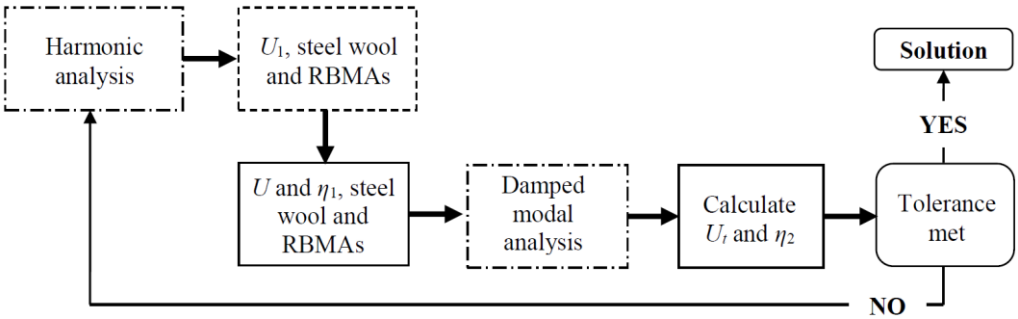


*Figure 9 – FE* (*dashed-dotted*) *and analytical* (*dashed*) *model cross-coupling process flow.*

### 3.1 Analytical model

The analytical model proposed represents the strain energy, $U_1$, for the RBMAs contained within the steel wool. When the steel wool is embedded with the RBMAs, the system behaves as an MDoF system with a set of tuned mass dampers (TMDs) as shown in Fig. 10.

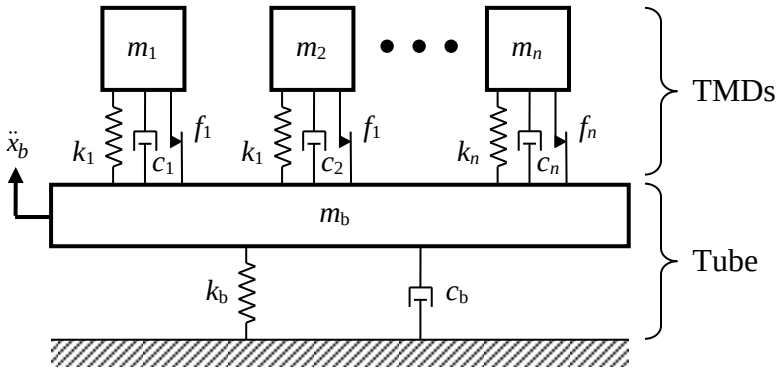


*Figure 10 – MDOF system for tube filled with steel wool and RBMAs.*

The stiffness of the steel wool does not vary greatly throughout its structure. For simplicity, in the analytical model it is assumed that these TMDs act in unison and therefore the vibrational damping is proportional to the summation of the peak dissipated energy from each RBMAs. The analytical model accounts for interaction between the RBMAs and the steel wool with the analogy of a sphere (RBMAs) and an elastic half-space (steel wool) as depicted in Fig. 11. Using a dimensionality reduction method, the model is represented as being a one-dimensional axisymmetric problem.

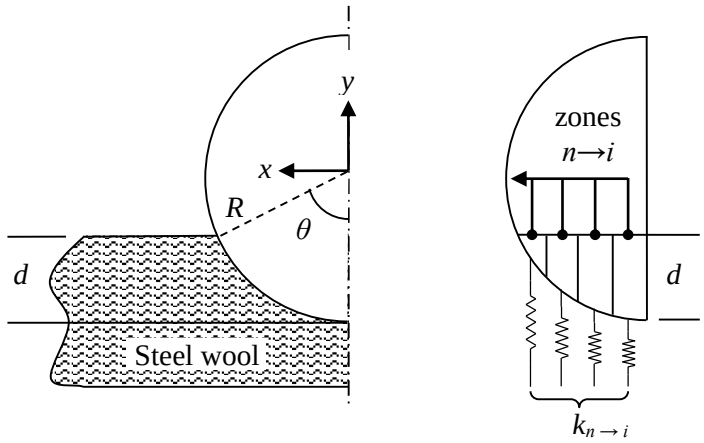


*Figure 11 – One-dimensional axisymmetric model for RBMA and steel wool for* (a) *RBMA and steel wool interaction and* (b) *stiffness representation for discretised zones.*

The model is based on the determining the force and displacement fields from the local deformation of the steel wool, caused by the RBMAs, whereby the strain energy can be evaluated. Four key assumptions apply to the model:

- RBMAs are spherical and rigid. The half-space has uniform homogeneous isotropic linear-elastic properties.
- RBMAs are far-field from one another and have no interacting contribution.
- RBMAs only provide movement normal to the steel wool.
- the deformation from the RBMAs in the steel wool only occurs directly under the RBMAs; no strain flow elsewhere.

To initiate the analytical model, an initial condition of a 'guessed' displacement is required. This displacement must be less than the radius of the RBMA. Using the initial deformation, $d$, the extreme angle, $\theta$, between the axisymmetric axis and the limited penetration, is described as

$$\theta = cos^{-1}\left[\frac{180(R-d)}{\pi R}\right], \tag{5}$$

where $R$ is the radius of the RBMA, $d$ is the deformation of the RBMA into the steel wool, $\pi$ is a mathematical constant, and *cos* is the cosine trigonometric function. To find the force and displacement of the curved surface, the discretised angle, $\theta_i$, is the ratio of the extreme angle to the number of substeps, $N$. Note that the subscript, $i$, refers to the iteration number. Once $\theta_i$ is defined, then the intersection point of the angle along the circumference needs to be estimated in Cartesian coordinates as

$$x_i = sin\left(\frac{\theta_i \pi}{180}\right)R, \tag{6}$$

$$y_i = \sqrt{R^2 - {x_i}^2}, \tag{7}$$

where $x_i$ and $y_i$ are the respective x and y coordinates. To estimate the stiffness of each discretised zone, bounded by the contiguous x and y coordinates, an effective length has be estimated which is described as

$$L_i' = \left[\left(x_i - x_{i-1}\right)\left(d - \left(R - y_i\right)\right)\right] + \left[\left(\left(\left(x_i - x_{i-1}\right)\left(y_{i-1} - y_i\right)\right)/2\right)/\left(x_i - x_{i-1}\right)\right]. \quad (8)$$

Each zone also covers an axisymmetrically discretised contact area between the RBMA and the steel wool. This area is described by

$$A_i = \left(\pi x_i^2\right) - \left(\pi x_{i-1}^2\right). \quad (9)$$

The force, $F$, acting on each zone, based on the amplitude of $d$, is described by

$$F = \sum_{i=1}^{n} \frac{A_i E L_i'}{t}, \quad (10)$$

where $E$ is the modulus of elasticity and $t$ is the thickness of steel wool in the direction of the acceleration. The amplitude of $F$ needs to be directly compared to that of the product of the acceleration (from the harmonic analysis) and the mass of the RBMA. If this amplitude varies from $F$, then the displacement, $d$, needs to be adjusted accordingly (if $d \uparrow$, then $F \uparrow$) until they agree within a tolerance. Once $F$ has converged to a solution, the average deformation of the steel wool can be estimated by weighting the $L_i'$ against the associated $A_i$. This is described by

$$D = \sum_{i=1}^{n} \left[ L_i' A_i \left( \sum_{i=1}^{n} A_i \right)^{-1} \right]. \quad (11)$$

Once $F$ and $D$ have been solved, the strain energy, $U_1$, can be calculated by

$$U_1 = \frac{FD}{2}. \quad (12)$$

One of the assumptions made with the analytical model is that the half-space is linear elastic. Dynamic mechanical tests were conducted on the steel wool to acquire both the model required input loss factor, $\eta$, and to determine the level of nonlinearity. From the model there is a nonlinearity that is caused by the change in deformation through the force and displacement fields created by the RBMAs. The nonlinearities for the steel wool and for the strain energy from the analytical model are shown in Figure 12.

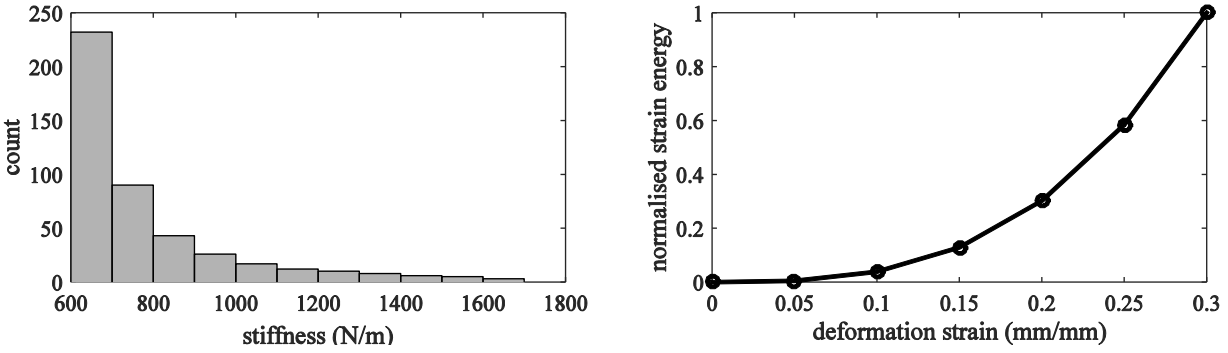


(a) (b)

*Figure 12 – Nonlinearity for* (a) *stiffness for extra fine steel wool and* (b) strain energy from the *analytical model for a 10mm diameter steel RBMA.*

The nonlinearity of the steel wool was considered from the start of loading until a maxima was reached in that loading direction to maximise the force-displacement nonlinear response. The force-displacement for this range had a sampling discretisation of 452 data points allowing for that many stiffness values to be calculated. Before calculating the stiffness, the data was ran through a second-order Savitzky-Golay filter to remove the measurement noise. The stiffness to use in the model was calculated by taking the first 5 bins from the histogram as it accounted for ~80% of the stiffness and each bin was weighted against its contribution to the total count of all the bins. The estimated stiffness used was 728Pa.

## 4 CONCLUSIONS

In this paper, several experiments were conducted and presented related to describing and demonstrating the effectiveness of using rigid body motion amplifiers (RBMAs) embedded in commercial fine grade steel wool. The results clearly identified that the RBMAs increased the level of damping significantly for mode 1 up to the order of 2328% with a small weight penalty of 3.8%. It was also shown that for mode 2 there were almost always an increase in damping from the RBMAs but this was not as significant as mode 1. Also presented was a semi-analytical numerical model in which can be used to describe the strain energy caused by a single RBMA. It does not go without saying that the model does however rely heavily on the material properties (stiffness) and characteristics (amplitude dependent vibrational loss factor) of the steel wool. These are essential inputs into the model and the process.

## REFERENCES


[1] Ma, Y., Tong, X., Lu, H., Zhang, D. & Hong, J. Investigation on fatigue life of metal rubber under alternating load, *proceedings from the International Conference on Experimental Mechanics*, Cambridge, United Kingdom, 2014.

[2] Ma, Y., Gao, D., Zhang, D. & Hong, J. Compressive and dissipative behaviour of metal rubber under constraints, *physica status solidi (b)*, 2015; 252(7).

[3] Yang, J., Xiong, Y. & Xing, J. Power flow behaviour and dynamic performance of a nonlinear vibration absorber coupled to a nonlinear oscillator, *Nonlinear Dynamics*, 2015; 80(3).

[4] Yang, J. *Power flow analysis of nonlinear dynamical systems*. University of Southampton, Faculty of Engineering and the Environment, Doctoral Thesis, 2013.